# Crack source location by acoustic emission monitoring method in RC strips during in-situ load test

Tala Shokri[*] and Antonio Nanni[a]

*College of Engineering (Civil), University of Miami, Coral Gables, USA*

**Abstract.** Various monitoring techniques are now available for structural health monitoring and Acoustic Emission (AE) is one of them. One of the major advantages of the AE technique is its capability to locate active cracks in structural members. AE crack locating approaches are affected by the signal attenuation and dispersion of elastic waves due to inhomogeneity and geometry of reinforced concrete (RC) members. In this paper, a novel technique is described based on signal processing and sensor arrangement to process multisensory AE data generated by the onset and propagation of cracks and is validated with experimental results from an in-situ load test. Considering the sources of uncertainty in the AE crack location process, a methodology is proposed to capture and locate events generated by cracks. In particular, the relationship between AE events and load is analyzed, and the feasibility of using the AE technique to evaluate the cracking behavior of two RC slab strips during loading to failure is studied.

## 1. Introduction

Acoustic Emission (AE) is defined as the release of transient elastic waves produced by a rapid redistribution of stress in a material. Within the family of non-destructive test methods, AE is classified as a passive technique providing capability to locate active cracks in structural members. AE crack locating approaches are affected by the signal attenuation and dispersion of elastic waves due to inhomogeneity and geometry of reinforced concrete (RC) members. AE methods of crack location are already well established in steel structures, but due to the heterogeneous nature of concrete, accuracy, identification, and attenuation of acoustic waves are still areas where development is desirable (Weiler *et al.* 1997).

This research is an attempt to relate the results obtained during a load test performed on two RC slab strips to the corresponding AE data in order to evaluate the application of the AE technique for determination of crack location and propagation in a concrete member. The experiments are performed in a three-story apartment building built in 1947 and scheduled for demolition. Two identical strips of a one-way RC slab of the first floor of the building are saw cut

---
[*]Corresponding author, Ph.D. Candidate, E-mail: t.shokri@umiami.edu
[a] Professor, E-mail:nanni@miami.edu

and loaded to failure. The AE signals reflecting the release of energy taking place during the damage process are recorded and by analyzing these recorded signals, cracks are located. In this paper, sources of uncertainty in the crack location approach are considered and a novel methodology to improve the accuracy of crack location results is presented. In this method, a sensor placement technique considering the signal attenuation and failure mechanism of the strips is introduced.

## 2. Research significance

The paper introduces a method to detect the onset and propagation of cracks and their location in a RC member using AE signals. For this method to be employable, a framework for data preparation and analysis including sensor arrangement, wave velocity optimization and data filtering is proposed.

## 3. Crack location method

AE is a phenomenon of transient stress waves resulting from a sudden release of elastic energy caused by mechanical deformations, initiation and propagation of microcracks, dislocation movement and other irreversible changes in material (ASTM E1316-05 2005). Sensors placed on the surface of structural members may be utilized to detect the acoustic waves produced by a source. A signal that exceeds a defined threshold is called "hit" and triggers the accumulation of data. If the same signal is recorded by more than one sensor, it is considered to be illustrative of a significant incident and called "event". If sufficient information about an individual event is obtained, the location of the AE source can be determined (Carpinteri *et al*. 2008).

The basis for the location calculation is the simple time-distance relationship implied by the velocity of the sound wave which is called point location. The absolute arrival time, *t*, of a hit in an event can be combined with the velocity of the sound wave, *v*, to yield the distance, *d*, from the sensor to the source

$$d = vt \tag{1}$$

In this formula, the velocity is constant and the distance $d_i$ between the source of unknown coordinates $(x_0, y_0, z_0)$ and sensor *i* with known coordinates $(x_i, y_i, z_i)$ can be found as (Miller and Mclntire 1987)

$$d_i = \sqrt{(x_i - x_0)^2 + (y_i - y_0)^2 + (z_i - z_0)^2} \tag{2}$$

The distance of the source to the sensor "*i*" can also be given by

$$d_i = v(t_i - t_0) \tag{3}$$

Where $t_i$ is the arrival time to sensor *i* and $t_0$ is the time of event occurrence.

This calculation is complicated by the lack of knowledge of the exact time the event originated. To get around this problem, all the times are considered relative to the first hit in the event. Each arrival time difference implies a difference in distance to the sensor relative to the distance to the first hit sensor (Shull 2002 and Salinas *et al*. 2010). For the second sensor, *i=2*, relative to the first sensor, *i=1*, a difference equation can be written as

$$t_2 - t_1 = (d_2 - d_1)/v \tag{4}$$

Considering a two-dimensional (plane) geometry, where $x_0$ *and* $y_0$ are the unknown coordinates of the source, Eq. (2) can be combined with Eq. (4) to yield

$$t_2 - t_1 = \left[\sqrt{(x_2 - x_0)^2 + (y_2 - y_0)^2} - \sqrt{(x_1 - x_0)^2 + (y_1 - y_0)^2}\right]/v \tag{5}$$

This equation contains two unknowns ($x_0$ and $y_0$) and cannot be solved by itself. To get a second equation with the same two unknowns, a third sensor should be added producing equation

$$t_3 - t_1 = \left[\sqrt{(x_3 - x_0)^2 + (y_3 - y_0)^2} - \sqrt{(x_1 - x_0)^2 + (y_1 - y_0)^2}\right]/v \tag{6}$$

These simultaneous equations can then be solved for $x_0$ *and* $y_0$. The math becomes more complicated when extended to three dimensions (volumetric), but the approach remains the same (AEwin Software User's Manual 2009).

The accuracy of AE location method in RC members is affected by several factors, including the heterogeneous nature of the material system. Even if a crack is located, the error can be large depending on the size of the tested structure and the distance of the sources to the sensors (Grosse and Ohtsu 2008). Moreover, in practical applications, crack location must be obtained from the useable portion of very large data set. The sources of crack location error are listed as follow.

Attenuation: Attenuation dampens a stress wave as the wave front propagates away from its origin and spreads over a larger volume. Attenuation of a body stress wave in an infinite medium causes the wave amplitude to decrease proportional to the distance from the wave source (Miller and Mclntire 1987). RC has unique characteristics due to heterogeneity, porosity and presence of steel reinforcement. Cracks dampen the progressing wave or, when wide enough, can become barriers to wave transmission. Besides internal damping, AE waves travelling in RC members can undergo reflection, scattering, mode conversion and diffraction, where all this influences the propagation of stress waves (Miller and Mclntire 1987). Therefore, attenuation is considered as having the major influence on the accuracy of data collected from RC members and should be determined prior to a test.

Sensor Number and Configuration: For a point source to be identified, signals must be detected by a minimum number of sensors: two for linear, three for planar, four for volumetric media. However, using more sensors than necessary, improves accuracy (Miller and Mclntire 1987). Also, source location accuracy is strongly affected by the relative position of sensors in a sensor array (Guratzsch and Mahadevan 2010). In general, the location accuracy is best in the area enclosed by the sensors and decreases as sources move outside this area (Tobias 1976 and Miller and Mclntire 1987).

Velocity: Accurate knowledge of wave velocity is critical for source location (Muhamad Bunnori *et al*. 2006) and, prior to any test, it has to be attained. For RC members in particular, wave velocity may not remain constant during the performance of a test as cracks develop as a function of the applied load.

Time of Arrival (TOA): Because of the presence of surfaces, several modes of wave propagation exist within a body. Compression (P) waves mostly are used to investigate the location of a source in three-dimensional (3D) media (Muhamad Bunnori *et al*. 2006 and Grosse and Finck 2006). In this case, the major error in source location is due to the miscalculated TOA of an AE hit. Estimating the correct TOA for the P wave is a challenge especially when a wave propagates through concrete. Literature shows that interpretation of AE data by an expert manually processing

the data and selecting the signal TOA can improve location accuracy significantly (Miller and Mclntire 1987). Although for large data set, this is not possible and automation is indispensable. The automatic determination of TOA can be based on a present threshold (in dB scale) which is specific to a particular material and transducer. TOA is calculated from the first signal excursion above the threshold. Therefore, the choice of the threshold value is crucial to the quality of the TOA selection and location results (Miller and Mclntire 1987).

Frequency Band: To lessen the effect of noise present in an AE signal, an appropriate frequency filter setting should be selected. Frequency filters are used to reduce low-frequency mechanical noise and high-frequency electronic noise. The correct choice of frequency band has a critical effect on the detection range of the sensor and the vulnerability of the setup to background noise.

## 4. Methodology of AE monitoring of cracks

In this study, the point location technique based on the differences in TOAs of the signals generated from the cracks and recorded by a number of sensors is used for crack location. However, recognizing the challenges of AE monitoring in RC members with the objective of crack location especially in a situation where thousands of events may be recorded, a simple location algorithm is not sufficient (Miller and Mclntire 1987). Consequently, to improve the precision of the crack location obtained with the equipment and methodology used, a procedure is suggested that consists in performing an AE pre-test aimed at establishing the following: attenuation curves and sensor arrangement (including sensor spacing, number and configuration), threshold, velocity, and frequency band selection.

## 5. Experimental observation and result

### 5.1 Geometries, material and instrumentation

The structure of interest consisted of a RC frame and infill masonry walls. To investigate the one-way RC slab behavior, two 30-inch (762-mm) wide strips were cut through one of the slabs of the building and load tested (Fig. 1).The relevant geometry and material properties of the RC slab are given in Table 1. The width of the strips is selected so that three reinforcing bars are included in the cross-section. The centerlines of the two slab strips are 5 ft (1.52 m) apart. For both slab strips, the test load is applied at two points placed at one-third of the total span. The load test is conducted using a push-down loading configuration. Fig. 2 shows a picture of the load test setup.

### 5.2 AE equipment

In this research, the PAC Sensor Highway II system (AEwin Software User's Manual 2009) equipped with R6I-AST resonance sensors is used for AE data collection. This system with 16 high-speed AE channels is designed for unattended and remote monitoring use, and includes AEWin software (AEwin Software User's Manual 2009) for data analysis. The R6I-AST resonance sensors have an operating frequency range of 40 - 100 kHz and a resonant frequency of 55 kHz. The "I" designation indicates that the sensor has a built-in 40 dB preamplifier. To ensure proper coupling of each AE sensor, a two-part epoxy contact agent is applied to connect the
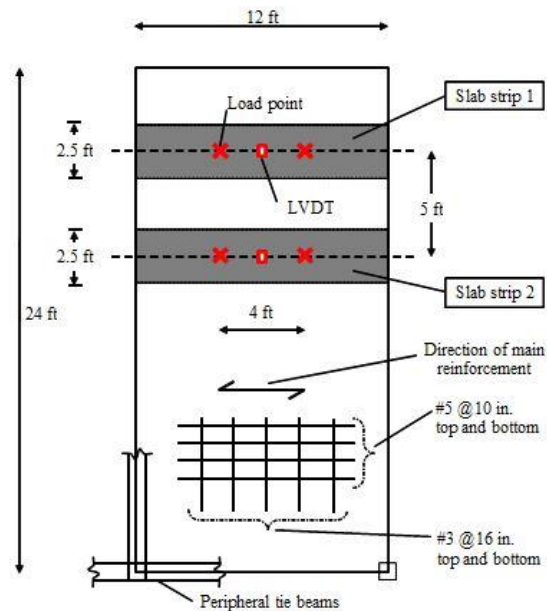
sensors to the concrete surface.



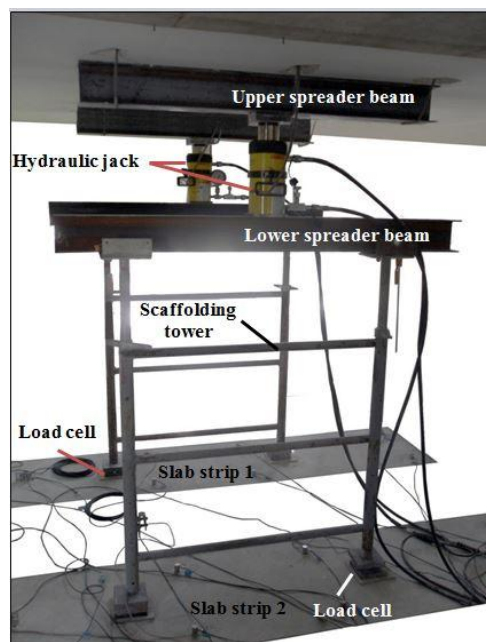Fig. 1 Slab strip layout. (Note: 1 in.=25.4 mm, 1ft=304.8 mm)



Fig. 2 Load test setup

Table 1 Summary of as built slab properties

| | |
|---|---|
| Short span | 12.0 ft (3.66 m) |
| Long span | 24.0 ft (7.32 m) |
| Thickness | 5.0 in. (127 mm) |
| Effective reinforcement depth (supports) | 3.75 in. (95.3 mm) |
| Effective reinforcement depth (mid-span) | 4.25 in. (104 mm) |
| Concrete strength | 3,000 psi (20 MPa) |
| Steel strength | 65,000 psi (448 MPa) |
| Main reinforcement[*,**] | #5@10 in. (16 @203 mm) |
| Secondary reinforcement[**] | #3@16 in. (9.5@406 mm) |

### 5.3 AE Pre-test

*Setup and Measurements.* The AE pre-test is performed on the slab in its original condition (pre-cut) by Pencil Lead Breaks (PLBs) at given locations to generate acoustic waves while the sensors are recording. PLB is an ASTM standard method to produce similar AE events (ASTM E 976-05 2005).The arrangement of the sensor for the AE pre-test (different from the one for the load test) is given in Fig. 3, which shows the location of five sensors with respect to the slab perimeter walls. Four sensors are placed in a rectangular fashion for the attenuation and wave propagation to be investigated in three directions. The fifth sensor is mounted at the center of this rectangle for location error considerations given that the proper arrangement of sensors requires equilateral triangle geometry (Vannoy *et al*. 1991). Using the standard 0.5 mm (0.019 in) diameter lead, PLBs are conducted at 3 in (76.2 mm) intervals between the sensors along the lines $S_1$-$S_2$; $S_1$-$S_3$; and, $S_1$-$S_4$. In order to minimize and uniformly distribute the operator errors, the PLBs are repeated three times at each position following a fully randomized order. The data is collected and analyzed before the load test.

*Data processing and results.* Fig. 4 shows the flow chart of the method of analysis for the AE pre-test that intends to reduce the location error. The following describes each column in the flow chart in more details together with experimental results.
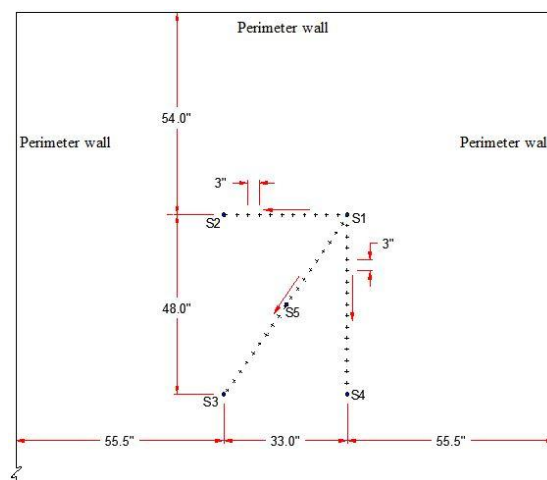


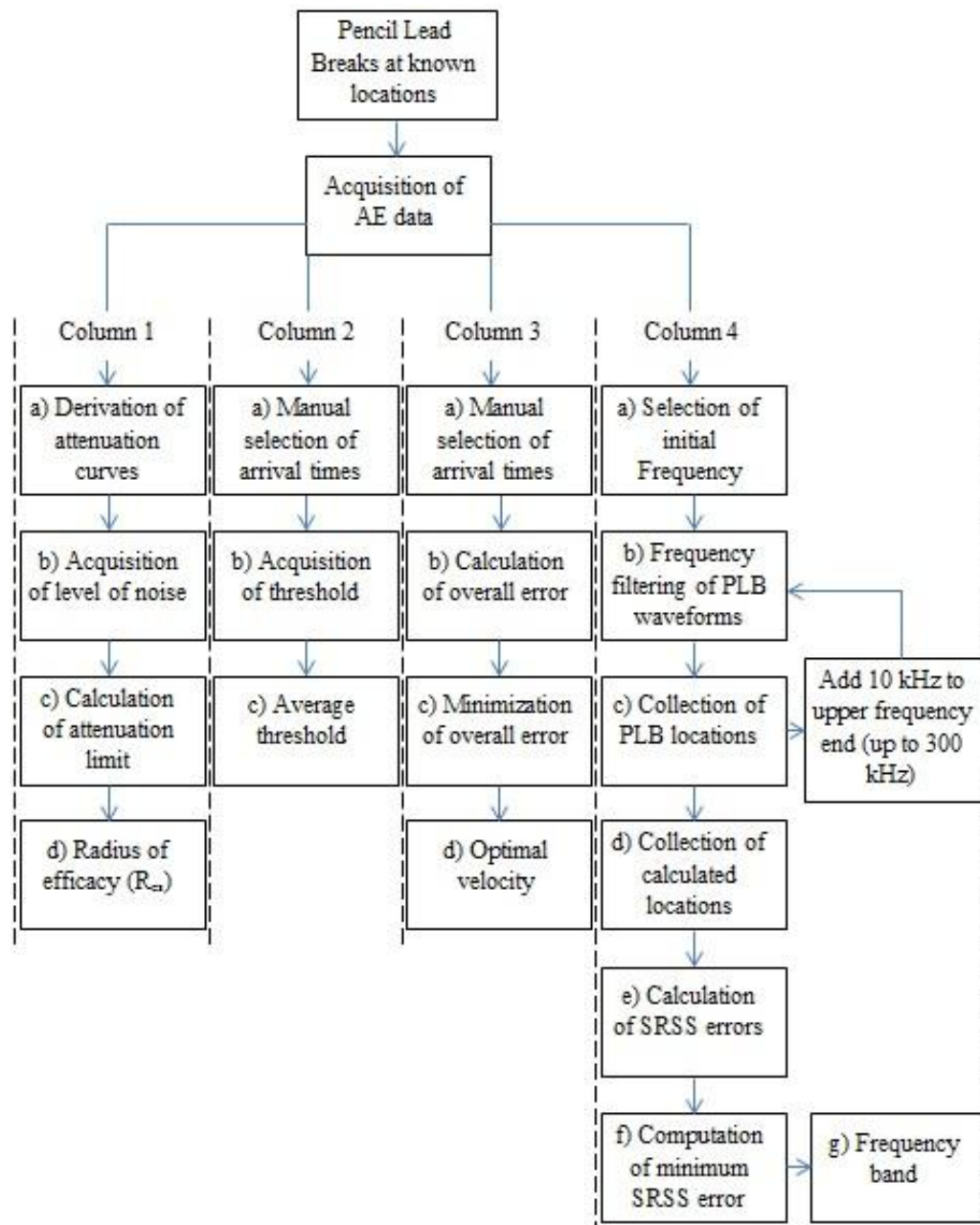Fig. 3 Paths and sensor setup for AE pre-test. (Note: 1 in.=25.4 mm)

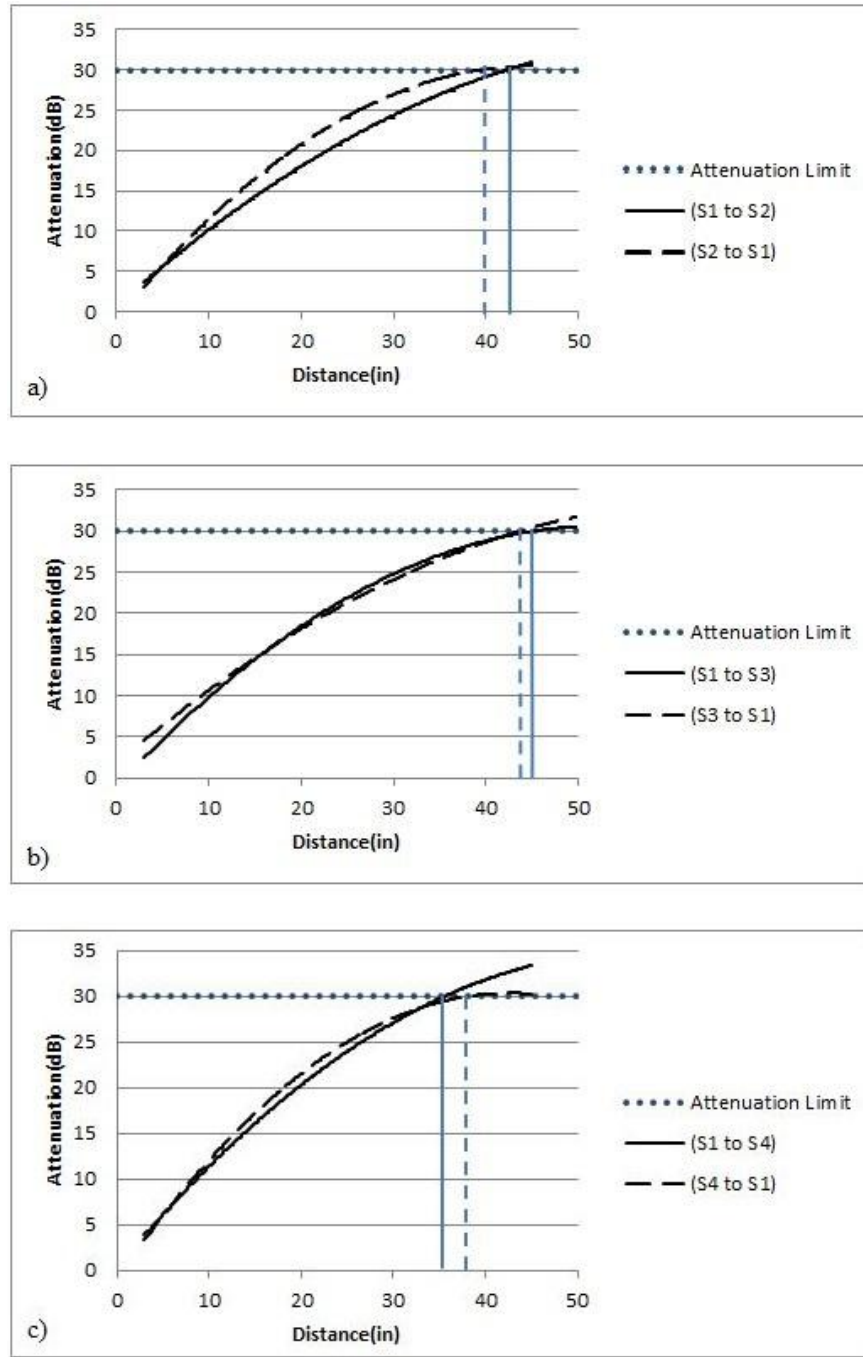Fig. 4 Method of analysis of AE pre-test data

*Tala Shokri and Antonio Nanni*



Fig. 5 Attenuation curves for selected paths: a) S1-S2 b) S1-S3 c) S1-S4. (Note: 1 in.=25.4 mm)

Column 1

This column consists of these steps:

a) Deriving attenuation curves for different directions

b) Obtaining the level of environmental noise amplitude

c) Deriving the attenuation limit

d) Finding the effective radius of efficacy ($R_{es}$) of a sensor

In step (a) of column 1, six attenuation curves shown in Fig. 5 are derived for three PLB paths of Fig. 3. For each line between sensors (three directions) two curves are obtained. Attenuation limits maximum sensor distance, which, consequently, limits the area that can be accurately monitored by a fixed number of sensors.

In step (b), the level of the environmental noise amplitude is measured by acquiring AE data for four hours after the PLB test and a maximum noise level of 60 dB is determined.

In step (c), the objective is to find "attenuation limit" above which recorded signals due to crack propagation would not be recognizable from the environmental noise. The maximum detectable amplitude for R6I sensors is 100 dB, corresponding to the amplitude of the amplified signal when it reaches 10 volts (saturation limit of the system). However, the goal is set for concrete cracks with source amplitudes over 90 dB to be detected. As a result, 30 dB (i.e., 90-60) is selected as the "attenuation limit" (Fig. 5).

In step (d), in order to optimize the positioning of the sensors, a case-dependent parameter termed Radius of Efficacy of Sensor ($R_{es}$) is introduced. $R_{es}$ is defined as the distance from a sensor within which no source of AE can be overshadowed by noise. This parameter plays a major role in arranging the sensors and is calculated from the attenuation curves considering the attenuation limit.

Since the $R_{es}$ is a scalar value to be effective in all directions, it is chosen from the path with the largest attenuation corresponding to the path $S_1$-$S_4$ (Fig. 5(c)) in this case. Accordingly, the distance of 35 in (0.89 m) corresponding to the attenuation limit of 30 dB, is set as the $R_{es}$. Therefore, the sensor arrangement for the load test should be designed in a way that at least four sensors enclose the area of expected damage using $R_{es}$ 35 in (0.89 m).

Column 2

Column 2 displays the procedure to find the proper post processing threshold to be applied for TOA selection of AE load test data. This column consists of these steps:

a) Selecting the arrival times of PLBs manually

b) Recording the corresponding thresholds for all arrival times

c) Calculating the average of all recorded thresholds

In step (a) of column 2, waveforms recorded from PLBs performed between the sensors (Fig. 3) are used for TOA selection. For each line (S1-S2, S1-S3, S1-S4), the arrival times of the PLBs located on that line to the end sensors are selected manually based on their waveforms.

In step (b), the corresponding threshold for each TOA is recorded.

In step (c), the average of all recorded thresholds, 34 dB, is chosen to be imposed to AE load test data in post processing step.

Column 3

Column 3 demonstrates the procedure to calculate the optimal wave velocity through the RC member under consideration. This column consists of these steps:

a) Selecting the arrival times manually

b) Defining the overall error based on calculated and known locations of the PLBs

c) Minimizing the overall error

d) Finding the optimal velocity

In step (a) of column 3, the manually picked arrival times, described in column 2 step a, are collected for velocity calculation.

In step (b) and (c) of column 3, the optimal velocity is defined so that the overall error, $E_D$, between the difference of calculated distances $\Delta d_j = (d_2 - d_1)_j$ of PLB $j$ to the end sensors and their actual values, $\Delta D_j = (D_2 - D_1)_j$, is minimized. For each break located between the sensors along the lines $S_1$-$S_2$, $S_1$-$S_3$, and $S_1$-$S_4$ (Fig. 3), $d_2$ and $d_1$ are the calculated distances of PLB $j$ to the end sensors and $D_2$ and $D_1$ are the exact distances. Defining the error as

$$E_D^2 = \sum_{j=1}^{n}\left(\Delta D_j - \Delta d_j\right)^2 = \sum_{j=1}^{n}\left(\Delta D_j - v\Delta t_j\right)^2 \tag{7}$$

Where $\Delta t_j = (t_2 - t_1)_j$ and manually picked arrival times of PLB $j$ to the end sensors can be used as $t_1$ and $t_2$. This can be minimized by

$$\frac{\partial E_D^2}{\partial v} = 0 \rightarrow \sum_{j=1}^{n}\Delta t_j\left(\Delta D_j - v\Delta t_j\right) = 0 \tag{8}$$

Resulting in the optimal velocity, $v$ of

$$v = \frac{\sum_{j=1}^{n}\Delta t_j \Delta D_j}{\sum_{j=1}^{n}\Delta t_j^2} \tag{9}$$

In step (d), by substituting all arrival times selected in step (a) and known location of PLBs in Eq. (9) the optimal velocity is calculated. As a result, the optimal velocity of 120,000 in/s (3048 m/s) is used for AE source location during the load test.


Column 4

To find the frequency band, an iterative procedure is developed. In this iterative procedure the low-frequency end is constant and the high-frequency end is changing. This procedure consists of these steps:

a) Uploading the PLBs data into AEWin software and setting the initial frequency band

b) Frequency filtering of PLBs waveforms

c) Calculating PLBs locations using filtered waveforms

I. Adding 10 kHz to the upper frequency end (up to 300 kHz)

II. Repeating steps (b) and (c)

d) Exporting all calculated locations of PLBs into a database

e) Calculating the square root of the sum of the squares (SRSS) error

f) Finding the minimum of SRSS errors

g) Finding the best frequency band

In step (a) of this procedure, the AE pre-test AE data including PLB waveforms is uploaded into AEWin software. Since sensor manufacturer recommends low-frequency end of 20 kHz in highly attenuating material (AEwin Software User's Manual 2009), the Low-frequency end is constant at 20 kHz. The initial high-frequency end is set at 100 kHz.

In step (b), using the frequency band, all the waveforms are filtered.

In step (c), AEwin point location build-in algorithm (AEwin Software User's Manual 2009) is operated to find the location of all PLBs. Referring to point location technique and Eqs. (5) and (6), for this algorithm to be applicable, the differences in TOAs of   signals recorded by sensors, wave

velocity and known location of sensors are needed. To attain that, the TOAs extracted from PLBs filtered waveforms recorded by all five sensors, known location of five sensors (Fig. 3) and the optimal velocity of 120,000 in/s (3048 m/s) are imposed to the location algorithm. The procedure in steps (b) and (c) iterates and in each iteration10 kHz (up to 300 kHz) is added to previous upper frequency end and new locations for PLBs are calculated.

In step (d), the calculated locations of PLBs, from all iteration, are exported to a Matlab program for error analysis.

In steps (e) and (f), the objective is to find the best frequency band based on the minimum error between exact and calculated location of PLBs. The collective (overall) error is defined as the SRSS of the distances of all PLBs (exact position) from their respective calculated location, or in mathematical terms

$$E_{XY}^2 = \sum_{j=1}^n \left[ \left( X_j - x_{cj} \right)^2 + \left( Y_j - y_{cj} \right)^2 \right] \tag{10}$$

Where $E_{XY}$ denotes the error, $(X_j, Y_j)$ the exact coordinates of the PLB $j$, $(x_{cj}, y_{cj})$ the computed coordinates and $n$ the number of PLBs. This program calculates the collective error for each repetition (frequency band). In step (g), the high-frequency end corresponding to the best result (minimum collective error), 150 kHz, is chosen as the selected high-frequency end. Therefore, 20-150 kHz frequency band is selected for the AE data analysis during the load test.

The AE pre-test necessary for all field applications produces the following parameters:
- $R_{es}$ (i.e., 35 in (0.89 m))
- Threshold (i.e., 34 dB)
- Velocity (i.e., 120,000 in/s (3048 m/s))
- Frequency band (i.e., 20-150 kHz)

## 5.4 Load test

*Loading procedure.* The load test is conducted according to the cyclic loading protocol described in ACI 437 (ACI 437R-03 2003). After conducting the cyclic load test, the slab strips are loaded to failure. This study only covers on the load testing to failure. The experimental and theoretical results of the cyclic load test are discussed by De Luca *et al*. (2011).

*AE Monitoring.* Due to the limited number of sensors that could be attached to the instrument (16 sensors in total) only eight sensors are used for each slab strip. The optimal position of the sensors is designed using AE pre-test data analysis. Since the test is carried out to ultimate failure, the area of interest is the mid span of the strips. Four sensors are assigned to the area between the load points. Recognizing that the $R_{es}$ of each sensor is 35 in (0.89 m), as many as four sensor could cover zone of concern where crack formation is predicted (Fig. 6). To reduce noise, two sensors at each end of the strips are used as guard sensors (i.e., sensors $S_1$, $S_2$, $S_7$ and $S_8$ (Fig. 6)). This is a noise rejection technique based on wave arrival times: if an AE wave is detected first by a guard sensor, it is ignored in the analysis as it is assumed that the source of the wave is outside the area of interest.

*Crack location procedure.* Fig. 7 presents the crack location procedure based on the outcome of the AE pre-test. This procedure consists of these steps:
a) AE recording
b) Extracting noise using guard sensors
c) Frequency filtering

d) Applying calculated threshold for TOA selection

e) Employing the wave velocity to the location algorithm

f) Locating the cracks

In step (a), the AE recording begins along with the load testing to failure and AE data is acquired continuously. In step (b), after conducting the load test, noise is extracted from the AE data using the guard sensors. In step (c), the data is filtered using frequency band of 20 kHz - 150 kHz.

In step (d), the TOAs of all hits are selected by applying calculated threshold of 34 dB on the filtered data. In step (e), the optimal velocity of 120,000 in/s (3048 m/s) is imposed to the AEwin point location built-in location algorithm.

At the end, in step (f), by knowing the exact location of the sensors, the wave velocity of signal through material and the time differences between the hits (Eqs. (5) and (6)), the events (cracks) are determined and AEwin point location built-in algorithm is operated to map the crack location. The two strips have almost identical behavior, thus only the results from strip 2 are presented here.
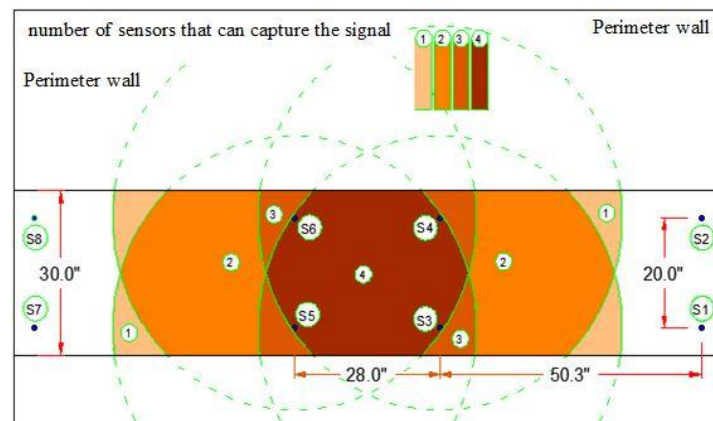


Fig. 6 Schematic map of locating capabilities and area of efficiency of the sensors for strip 2

*Results and Discussion.* By applying the procedure described in Fig. 7, events generated from the cracks are captured and located after they occurred in midspan of strip. This allows for the monitoring of crack formation and comparison with visible cracks on the surface during the load test.

In a sequence, the recorded AE events at the midspan during three load segments from 0-9000 lb (40.0 kN) are shown in Fig. 8. Theoretical calculation shows that the midspan is expected to crack when load reaches 3000 lb (13.3 kN) (De Luca *et al.* 2011). In order to indicate the crack initiation at midspan, the first segment is chosen to cover loading up to 3500 lb (15.6 kN) just above anticipated theoretical midspan cracking load. Loading from 3500 lb (15.6 kN) to failure (9000 lb (40.0 kN)) then is split into two segments for purpose of clarity of analysis. The number of AE events at midspan increases considerably when the load approaches 3100 lb (13.8 kN) (Fig. 8(a)) indicating crack initiation at midspan. Fig. 8(b) shows an increase in the AE event rate, as cracks continue to propagate and form. The last stage (Fig. 8(c)) produces the largest number of events, which is due to the crack extending and spreading in the center portion of the strip.
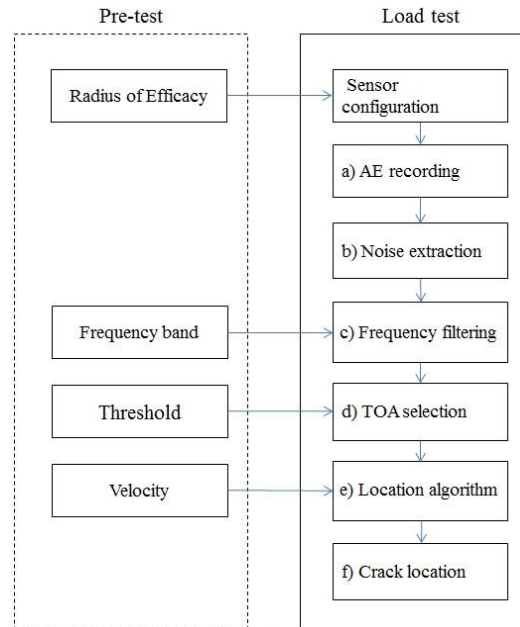
Fig. 7 Flow chart of the method of crack location during a load test

Using the AE data between 0 to 9000 lb (40.0 kN) load levels, the cracks (events) identified under the load test are located and an AE crack map for the midspan region is developed. Fig. 9 shows the crack evolution during the loading process. For each load segment, the AE estimated source location of the cracks in the X-Y plane are visualized from the bottom and compared with a picture of cracks taken during the load test (Fig. 9). The location of AE sources is marked with a square and each circle represents the location of a sensor. The pictures taken in the field are not to scale and cracks lines are manually accentuated on visible cracks for purpose of clarity. As seen in Fig. 9, located AE events correspond closely to the locations of visible cracks, and often precede their appearance. For instance, in Fig. 9(a) there are cracks located on the right side of sensors 3 and 4 in the AE map which were not visible during the load test in this stage, but later by increasing the load they became visible (Fig. 9(b)).This comparison shows the ability of AE location technique to identify and locate cracks at early stage before they become visible. In Fig. 9 the accuracy of crack location varies because of two important limitations:

- The presence of cracks affects the velocity of waves traveling from source to sensors.
- The area enclosed by the sensors does not entirely cover the area affected by cracks.

During the test, crack initiation and propagation create barriers for wave to travel across the cracks. Therefore, a wave travels a longer path to reach the sensors and this changes the effective velocity from source to sensor and directly affects the accuracy of crack location. By introducing the optimal velocity, the error is significantly reduced, but velocity changes during the test and earlier cracks are more precisely located than the final stage cracks. This uncertainty can be seen in Fig. 9(c) where the cracks on the left side of sensors 5 and 6 are not as clear as earlier cracks. Accuracy of location at all stages of the test can be maintained and improved by introducing variable velocity.
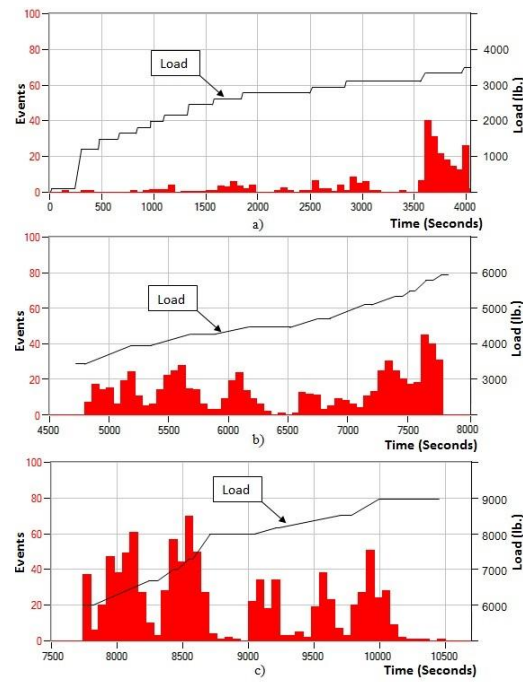
Fig. 8 Events vs. time at midspan for loading from : (a) 0 to 3500 lb, (b) 3500 to 6000 lb and (c) 6000 to 9000 lb. (Note: 1,000 lb=4.448 kN)
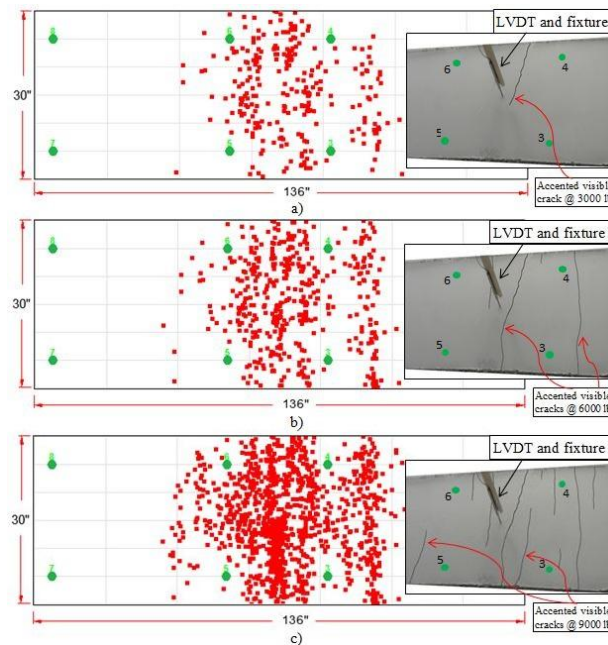


Fig. 9 Mid-span crack location for loads up to: (a) 3500 lb, (b) 6000 lb and (c) 9000 lb. (Note: 1,000 lb=4.448 kN, 1in.=25.4 mm)

The location accuracy is best in the area enclosed by the sensors and decreases as sources move outside this area. Due to the limited number of sensors and material attenuation, only the center part of the strip (Fig. 6) could be covered with the enclosed array of the sensors, thus affecting accuracy outside this area (Fig. 9(c)). It should be noted that if the crack occurring outside of enclosed area of the sensors has high source amplitude and energy, it can still be located with good precision (Fig. 9(c)). The results shown in Fig. 9 demonstrate that the proposed approach has the potential for AE crack detection and location in RC members even with a limited number of sensors and simplifying assumptions.

## 6. Conclusions

The load test was performed on one way slab strips and the formation and propagation of cracks was observed. A methodology based on error minimization was proposed to capture and locate cracks using correlated AE events. As a result, a number of events highlighting the crack pattern was calculated and mapped. The methodology can be routinely used as pre-test before load testing on RC slabs. Approaches for establishing sensor arrangement, TOA selection, velocity optimization and data filtering were introduced. Sequence of controlled crack propagation, in RC strips was observed and the AE technique was able to locate the cracks with limited number of sensors (i.e., eight per strip) while they were forming and in some cases before they were visible. The pattern of the located AE events was consistent with the analytical calculations and experimental outcomes. The results show that this method has the potential to be a component of a structural load testing.

Additional research is necessary to introduce variable velocity in each stage of the load test for crack location. In addition, future work needs to develop a pattern recognition technique which can automatically recognize and draw the crack lines directly from the AE point locations.

## Acknowledgements

## References

ACI 437R-03 (2003), *Strength evaluation of existing concrete buildings*, ACI, Farmington Hills, MI.
AEwin Software User's Manual (2009), *Physical acoustic corporation*, Princeton Junction, NJ.
ASTM E1316-05 (2005), *Standard terminology for non destructive examination*, ASTM International, PA.
ASTM E976-05 (2005), *Standard guide for determining the reproducibility of acoustic emission sensor response*, ASTM International, PA.
Baron, J. and Ying, S. (1987), *Acoustic emission source location*, (Eds. R. Miller and P. McIntire), Nondestructive Testing Handbook Second Edition, Vol. 5: Acoustic Emission Testing, American Society for Nondestructive Testing.

Carpinteri, A., Lacidogna, G. and Manuello, A. (2008), *Localization accuracy of microcracks in damaged concrete structures*, Acoustic Emission and Critical Phenomena, Taylor & Francis Group, London.

De Luca, A., Zadeh, J.H. and Nanni, A. (2011), "In-situ load testing: assessment of the one way performance of reinforced concrete slabs", *Accepted for publication by ACI Structural Journal.*

Grosse, C.U. and Ohtsu, M. (2008), *Acoustic emission testing*, Springer.

Grosse, C.U. and Finck, F. (2006), "Quantitative evaluation of fracture processes in concrete using signal-based acoustic emission techniques", *Cement Concrete Comp.*, **28**, 330-336.

Guratzsch, R.F. and Mahadevan, S. (2010), "Structural health monitoring sensor placement optimization under uncertainty", *AIAA J.*, **48**(7), 1281-1289.

McLaskey, G.C. and Glaser, S.D. (2007), "Temporal evaluation and 3D location of acoustic emission produced from the drying shrinkage of concrete", *Adv. Acoust. Emission J.*, **6**, 52-57.

Miller, R.K. and Mclntire, P. (1987), *Non-destructive testing handbook*, Vol. 5, Acoustic Emission Testing, American Society for Nondestructive Testing, USA.

Muhamad Bunnori, M., Pullin, R., Holford, K.M. and Lark, R.J. (2006) "A practical investigation into acoustic wave propagation in concrete structures", *Adv. Mater. Res. J.*, **13-14**, 205-212.

Ohtsu, M., Uchida, M., Okamoto, T. and Yuyama, S. (2002) "Damage assessment of reinforced concrete beams qualified by acoustic emission", *ACI Struct. J.*, **99**(4), 411-417.

Salinas, V., Vargasa, Y., Ruzzanteb, J. and Gaetea, L. (2010), "Localization algorithm for acoustic emission", *Phys. Procedia*, **3**, 863-871.

Shull, P.J. (2002), *Nondestructive evaluation theory*, Techniques, and Applications, Marcel Dekker Inc, New York, NY.

Tobias, A. (1976), "Acoustic emission source location in two dimensions by an array of three sensors", *Non-Destructive Testing*, **9**(1), 9-12.

Vannoy, D.W., Hariri, R. and Frantzis, C.D. (1991), *Acoustic emission investigation and signal discrimination in highway bridge applications*, Research report, Maryland State Highway Administration, FHWA/MD-91/05.

Weiler, B., Xu, S.L. and Mayer, U. (1997), "Acoustic emission analysis applied to concrete under different loading conditions", *Otto Graf J.*, **8**, 255-272.

*BS*

## Notations

$D_i$: known distance between sensor $i$ and the source
$d_i$: calculated distance between sensor $i$ and the source

$E_D$: overall error

$E_{XY}$: minimum square root of the sum of the squares error

$n$: number of artificially created sources (PLBs)

$R_{es}$: radius of efficacy of sensors

$t_0$: time of event occurrence

$t_i$: arrival time to sensor $i$

$v$: velocity of the acoustic wave

$X_j$: exact $x$ coordinate of the PLB $j$

$x_0$: unknown $x$ coordinate of the source

$x_{cj}$: computed $x$ coordinate of the PLB $j$

$x_i$: known $x$ coordinate of sensor $i$

$Y_j$: exact $y$ coordinate of the PLB $j$

$y_0$: unknown $y$ coordinate of the source

$y_{cj}$: computed $y$ coordinate of the PLB $j$

$y_i$: known $y$ coordinate of sensor $i$

$z_0$: unknown $z$ coordinate of the source

$z_i$: known $z$ coordinate of sensor $i$

$\Delta D_j$: difference of exact distances of PLB $j$ to the end sensors

$\Delta d_j$: difference of calculated distances of PLB $j$ to the end sensors

$\Delta t_j$: difference of arrival time of PLB $j$ to the end sensors